Platinum-Containing Hyper-Cross-Linked Polystyrene as a Modifier-Free Selective Catalyst for L-Sorbose Oxidation

S. N. Sidorov,[†] I. V. Volkov,[†] V. A. Davankov,[†] M. P. Tsyurupa,[†] P. M. Valetsky,[†] L. M. Bronstein,*[,‡] R. Karlinsey,[‡] J. W. Zwanziger,[‡] V. G. Matveeva,[§] E. M. Sulman,[§] N. V. Lakina,[§] E. A. Wilder,[⊥] and R. J. Spontak*[,⊥]

Contribution from the Nesmeyanov Institute of Organoelement Compounds, Moscow 117813, Russia, Department of Chemistry, Indiana University, Bloomington, Indiana 47405, Tver Technical University, Tver 170000, Russia, and Departments of Chemical Engineering and Materials Science & Engineering, North Carolina State University, Raleigh, North Carolina 27695

Received March 26, 2001

Abstract: Impregnation of hyper-cross-linked polystyrene (HPS) with tetrahydrofuran (THF) or methanol (ML) solutions containing platinic acid results in the formation of Pt(II) complexes within the nanocavities of HPS. Subsequent reduction of the complexes by H_2 yields stable Pt nanoparticles with a mean diameter of 1.3 nm in THF and 1.4 nm in ML. The highest selectivity (98% at 100% conversion) measured during the catalytic oxidation of L-sorbose in water is obtained with the HPS-Pt-THF complex prior to H_2 reduction. During an induction period of about 100 min, L-sorbose conversion is negligible while catalytic species develop in situ. The structure of the catalyst isolated after the induction period is analyzed by X-ray diffraction, transmission electron microscopy, and X-ray photoelectron spectroscopy. Electron micrographs reveal a broad distribution of Pt nanoparticles, 71% of which measure less than or equal to 2.0 nm in diameter. These nanoparticles are most likely responsible for the high catalytic activity and selectivity observed. The formation of nanoparticles measuring up to 5.9 nm in diameter is attributed to the facilitated intercavity transport and aggregation of smaller nanoparticles in swollen HPS. The catalytic properties of these novel Pt nanoparticles are highly robust, remaining stable even after 15 repeated uses.

Introduction

Noble metal nanoparticles formed in various media and stabilized by different mechanisms remain a subject of intense study due to their promising catalytic properties, which are often superior to those of traditional heterogeneous catalysts.[1−4] Polymers in solutions and in bulk are often employed to stabilize such nanoparticles. Over the past few years, reports of controlled nanoparticle formation in nanostructured polymeric media, especially macromolecular surfactants, have appeared.[5−11] Amphiphilic block copolymer micelles in selective solvents, for instance, can be used to control the size, size distribution, shape, and morphology of nanoparticles. The tailored synthesis of well-defined amphiphilic block copolymers is, however, extremely demanding due to the required purity of all the reactant species. This practical shortcoming drives the ongoing search for more robust and inexpensive polymeric matrices exhibiting nanostructures that function in both aqueous and organic media. One such matrix is hyper-cross-linked polystyrene (HPS).[12,13] Due to its high cross-link density, which can exceed 100%, HPS consists of nanosized rigid cavities of comparable size in the 2−3 nm range. It is readily produced by chemically incorporating methylene groups between adjacent phenyl rings in dissolved polystyrene homopolymer or gelled poly(styrene-*r*-divinylbenzene) copolymer in the presence of ethylene dichloride. Good solvent and conformational network rigidity are generally necessary to prepare hyper-cross-linked polymers possessing extremely high inner surface areas (typically in the range of 1000 m^2/g). In the present study, we use HPS with the following characteristics: (i) a formal degree of cross-linking of 200%, (ii) an apparent inner surface area of 833 m^2/g, (iii) a sharp pore size distribution maximum at about 2 nm in diameter, and (iv) particle sizes ranging from 0.2 to 0.4 mm in diameter.

A unique feature of HPS is its ability to swell in a wide variety of different solvents, even thermodynamically poor ones (e.g., water). Such versatility greatly facilitates incorporation of various organometallic compounds into the nanostructured

* To whom correspondence should be addressed.
[†] Nesmeyanov Institute of Organoelement Compounds.
[‡] Indiana University.
[§] Tver Technical University.
[⊥] North Carolina State University.

(1) Schmid, G., Ed. *Clusters and Colloids*; VCH: Weinheim, Germany, 1994.
(2) Baiker, A.; Grunwaldt, J.-D.; Müller, C. A.; Schmid, L. *Chimia* **1998**, *52*, 517.
(3) Bradley, J. S. *Schr. Forschungszent. Jülich, Mater.* **1998**, 1 (Physik der Nanostrukturen), D6.1.
(4) Bönnemann, H.; Braun, G.; Brijoux, W.; Brinkmann, R.; Tilling, A. S.; Seevogel, K.; Siepen, K. *J. Organomet. Chem.* **1996**, *520*, 143.
(5) Antonietti, M.; Wenz, E.; Bronstein, L.; Seregina, M. *Adv. Mater.* **1995**, *7*, 1000.
(6) Chan, Y. N. C.; Schrock, R. R.; Cohen, R. E. *Chem. Mater.* **1992**, *4*, 24.
(7) Chan, Y. N. C.; Craig, G. S. W.; Schrock R. R.; Cohen, R. E. *Chem. Mater.* **1992**, *4*, 885.
(8) Saito, R.; Okamura, S.; Ishizu, K. *Polymer* **1992**, *33*, 1099. Saito, R.; Okamura, S.; Ishizu, K. *Polymer* **1993**, *34*, 1183, 1189.
(9) Moffitt, M.; McMahon, L.; Pessel, V.; Eisenberg, A. *Chem. Mater.* **1995**, *7*, 1185.
(10) Spatz, J. P.; Roescher, A.; Möller, M. *Adv. Mater.* **1996**, *8*, 337.
(11) Bronstein, L. M.; Chernyshov, D. M.; Valetsky, P. M.; Wilder, E. A.; Spontak, R. J. *Langmuir* **2000**, *16*, 8221.
(12) Davankov, V. A.; Tsyurupa, M. P. *React. Polym.* **1990**, *13*, 27.
(13) Tsyurupa, M. P.; Davankov, V. A. *J. Polym. Sci.: Polym. Chem. Ed.* **1980**, *18*, 1399.

10.1021/ja0107834 CCC: $20.00
Published on Web 10/05/2001

Scheme 1

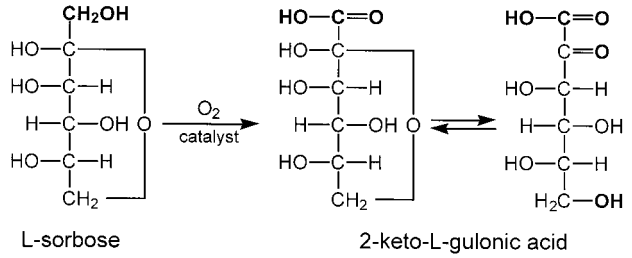

HPS matrix. A preceding study[14] addressing the formation of Co nanoparticles in HPS has demonstrated that the HPS cavities effectively restrict metal nanoparticle growth, thereby providing precise control over particle size and shape. On the basis of these results, we have surmised that this polymer matrix could also be used to control the formation of noble metal nanoparticles prepared upon reduction of precursor metal complexes,[11] thus expediting the development of new nanocomposite systems with interesting catalytic properties. Moreover, since HPS swells in most solvents, access of reactant species to catalytic sites in a self-supporting substrate would be provided in virtually any reaction medium.

In the present work, we examine the incorporation of H_2PtCl_6 in HPS and the subsequent formation and catalytic property development of Pt nanoparticles. An example of a catalytic reaction of fundamental, as well as technological, interest is the oxidation of L-sorbose to 2-keto-L-gulonic acid. Several strategies based on chemical, electrochemical, biotechnological, and catalytic methods are currently available for the oxidation of this ketose, which serves as an intermediate in Vitamin C production. While the catalytic route promises to be the most viable, it has been thwarted by complications. Due to acetonation, carbohydrate functional groups are initially protected from oxidation, in which case the reaction selectivity increases. The initial functional groups must, however, be recovered after oxidation, resulting in tremendous loss of end-product.[15,16] Direct catalytic oxidation of L-sorbose to 2-keto-L-gulonic acid by the reaction[17−20] displayed in Scheme 1 avoids acetonation altogether. This reaction has been performed in the presence of O_2 over a Pt or Pd catalyst deposited on activated carbon or aluminum oxide. In this case, the reaction must be conducted in neutral or low-alkali media. Selectivity may be increased through the addition of modifying (promoting) agents such as phosphine and aminophospine complexes, as well as aromatic and cycloaliphatic amines, at optimal loading levels. The resultant selectivity unfortunately decreases from 95% at 30% conversion to 40% at 100% conversion. Thus, the two principal disadvantages of this procedure are (i) low selectivity at high conversion and (ii) contamination of the end-product with reaction modifiers. The present work details the synthesis of a modifier-free catalyst based on Pt-containing HPS, which exhibits both high catalytic activity and selectivity in the oxidation of L-sorbose.

Scheme 2

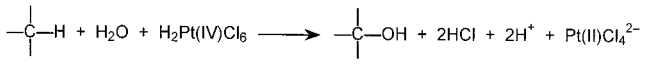

Results and Discussion

Characteristics of HPS-Pt Nanocomposites. Incorporation of Pt complexes into the nanostructured matrix of HPS is achieved by swelling HPS particles in the presence of THF or ML solutions containing H_2PtCl_6. During solvent removal under vacuum at ambient temperature, the color of the HPS powder changes for samples prepared in THF (HPS-Pt-THF) and ML (HPS-Pt-ML) solutions. This color change is inferred to be indicative of a chemical transformation in the functionality of the Pt compound. As reported earlier,[21,22] impregnation of H_2PtCl_6 into carbon and pregraphitized carbon black in the presence of water promotes the reduction of Pt(IV) to Pt(II), along with the simultaneous oxidation of the carbon, as depicted in Scheme 2. The detailed mechanism by which Pt(IV) is reduced and carbon is oxidized is discussed elsewhere.[22] In the present work, we presume that HPS can be envisaged as pregraphitized carbon containing both arene cycles and CH groups, and should therefore induce the same chemical response elicited by the reaction shown in Scheme 2.

According to XPS data collected from both HPS-Pt-THF and HPS-Pt-ML samples, the binding energy of Pt $4f_{7/2}$ in each material is virtually identical at 73.6 ± 0.1 eV, which is measurably lower than that of Pt(IV). For comparison, the tabulated Pt $4f_{7/2}$ binding energy ranges for $K_2Pt(IV)Cl_6$, $K_2Pt(II)Cl_4$, and Pt(0) are 74.1−74.3, 72.8−73.4, and 71.0−71.3 eV, respectively. On the basis of these data, it is reasonable to conclude that H_2PtCl_6 undergoes a chemical transformation within the HPS matrix, resulting in the reduction of Pt(IV) to Pt(II). Deconvolution of the XPS spectra presented in Figure 1 reveals that almost all the Pt(IV) is reduced to Pt(II) in the HPS-Pt-THF sample (Figure 1a), whereas a residual fraction of Pt-(IV) remains in the HPS-Pt-ML sample (Figure 1b).

Compositional data acquired from elemental analysis of HPS and its Pt derivatives are presented in Table 1. Inconsistency in the overall composition makeup of HPS (the compositions sum to only 98.72 wt %) is attributed to the presence of a small amount of oxygen-containing groups, which account for about 1.3 wt % oxygen. Solid-state ^{13}C NMR spectra (Figure 2) have been collected from these materials under magic angle spinning (MAS) conditions with cross polarization. The ^{13}C MAS spectrum of metal-free HPS (Figure 2a) primarily shows signals arising from di- and trisubstituted arenes (at 125−140 ppm), as well as from CH and CH_2 groups (at 42 ppm). The corresponding FTIR spectrum of metal-free HPS displays several prominent signals that are inconsistent with the idealized model in which HPS consists of only CH and CH_2 groups and 1,2,3-substituted phenyl rings. These include a signal located at 910 cm^{-1}, as well as a weaker one at 990 cm^{-1}, both of which can be assigned to $-CH{=}CH_2$ groups.

Incorporation of Pt into HPS is accompanied by a measurable increase in oxygen content: up to 2.82 wt % in HPS-Pt-THF and 4.49 wt % in HPS-Pt-ML (see Table 1). The solid-state ^{13}C NMR spectrum of the HPS-Pt-THF material is presented in Figure 2c and exhibits a new signal (relative to the metal-

(14) Sidorov, S. N.; Bronstein, L. M.; Davankov, V. A.; Tsyurupa, M. P.; Solodovnikov, S. P.; Valetsky, P. M.; Wilder, E. A.; Spontak, R. J. *Chem. Mater.* **1999**, *11*, 3210.
(15) Lyazidi, H. A.; Benabdallah, M. Z.; Berlan, J.; Kot, C.; Fabre, P.-L.; Mestre, M.; Fauvarque, J.-F. *Can. J. Chem. Eng.* **1996**, *74*, 405.
(16) Cognet, P.; Berlan, J.; Lacoste, G.; Fabre, P.-L.; Jud, J.-M. *J. Appl. Electrochem.* **1995,** *25*, 1105.
(17) Mallat, T.; Brönnimann, C.; Baiker, A. *Appl. Catal. A−Gen.* **1997**, *149*, 103.
(18) Mallat, T.; Brönnimann, C.; Baiker, A. *J. Mol. Catal. A−Chem.* **1997,** *117*, 425.
(19) Brönnimann, C.; Bodnar, Z.; Aeschimann, R.; Mallat, T.; Baiker, A. *J. Catal.* **1996,** *161*, 720.
(20) Brönnimann, C.; Mallat, T.; Baiker, A. *J. Chem. Soc.−Chem. Commun.* **1995**, 1377.
(21) van Dam, H. E.; van Bekkum, H. *J. Catal.* **1991**, *131*, 335.
(22) Coloma, F.; Sepúlveda-Escribano, A.; Fierro, J. L. G.; Rodríguez-Reinoso, F. *Langmuir* **1994**, *10*, 750.

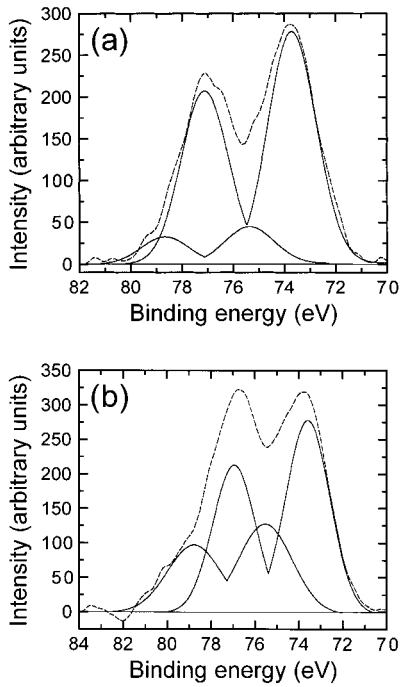

Figure 1. X-ray photoelectron spectra of (a) HPS-Pt-THF and (b) HPS-Pt-ML obtained with Mg Kα radiation. The experimental data are displayed as dashed lines, whereas deconvolution fits are shown as solid lines.

Table 1. Elemental Analysis Results from HPS and Its Pt Nanocomposites

	composition (wt %)			
designation	H	C	Cl	Pt
HPS	7.95	90.47	0.30	−
HPS-Pt-THF	7.28	77.71	4.68	7.51
HPS-Pt-ML	6.90	74.66	5.60	8.35

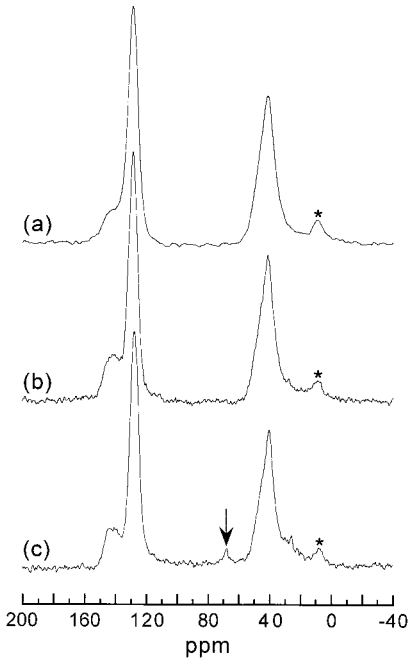

Figure 2. Solid-state ^{13}C NMR spectra of (a) HPS, (b) HPS-Pt-ML, and (c) HPS-Pt-THF. The asterisks identify spinning sidebands.

free HPS in Figure 2a) at 69 ppm, which can be assigned to either ether or hydroxyl groups. To elucidate the source of these oxygen-containing moieties, we have subjected the HPS-Pt-THF sample to THF extraction for 2 h under agitation, which yielded a dark brown THF solution that was subsequently evaporated and dried in vacuo (1 mbar) at ambient temperature. The FTIR spectrum of the resultant extract in the range of 400−250 cm^{-1} (the far-infrared) reveals two signals at 330 and 305 cm^{-1}. On the basis of their intensity and position, they are assigned to the $[PtCl_3L]^-$ ion, where L denotes the ligand.[23] A counterion should be $[H_3O]^+$. Note that similar signals are observed in the spectrum of HPS-Pt-THF. Several ligand structures can be hypothesized. According to XPS data, the platinic acid used throughout this study contains a small concentration of Pt(II) species. Labinger et al.[24] and Sen et al.[25] report that a mixture of Pt(IV) and Pt(II) compounds actively catalyzes THF oxidation in the presence of water (in our case, the source of water is $H_2PtCl_6 \times 6H_2O$). Upon doing so, several side products are obtained, including those shown below.[26] Moreover, the formation of alkyl chlorides due to the oxidation of alkanes by Pt compounds has also been demonstrated.[24] From these prior findings, we expect that γ-butyrolactone (GBL), a major product of this reaction,[25,26] will transform to the enole form, which is stabilized by coordination with $PtCl_3$ species. In this scenario, Pt(IV) is reduced to Pt(II).

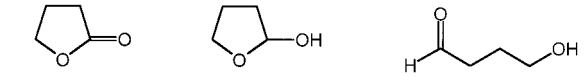

Another possibility to be considered is the coordination of GBL through its keto-group, although such complexes with $PtCl_3$ fragments have not been previously reported. The FTIR spectrum of the THF extract of HPS-Pt-THF shows signals at 3437 and 1178 cm^{-1} (characteristic of hydroxyl groups), 1625 cm^{-1} (water), 641 cm^{-1} (C−Cl groups), 1028 cm^{-1} (cyclic compounds), and others. Thus, we conclude that the reaction mixture resulting from interaction of THF with $H_2PtCl_6 \times 6H_2O$ contains several products, while free GBL in its keto-form is not present (the identifying strong signal at 1770 cm^{-1} is absent). Since all the possible side products possess high boiling temperatures (in the range of 180−203 °C), it is conceivable that their evaporation under vacuum at ambient temperature may be incomplete.

To confirm the formation of these side products, we have reacted $H_2PtCl_6 \times 6H_2O$ with THF for 24 h and recorded FTIR spectra at different stages of product drying. The formation of an orange-brown product accompanied by HCl evolution is already detectable only 2 h after $H_2PtCl_6 \times 6H_2O$ loading. The FTIR spectrum, recorded after the reaction was complete (in 24 h) and purged with Ar to remove THF, exhibits strong signals at 3401, 2942, 2870, 1106, 1051, and 1015 cm^{-1}, as well as moderate signals at 1733, 1635, 1444, 1388, and 647 cm^{-1}. Comparison of these FTIR spectral features with the IR signatures[27] of the compounds presumed to be present in the mixture (assuming GBL exists as enole), as well as with the spectrum of the THF extract, confirms the presence of oxidation products and provides evidence that is consistent with the reaction route described above. Thus, the interaction of H_2PtCl_6

(23) Goodfellow, R. J.; Goggin, P. L.; Duddell, D. A. *J. Chem. Soc. (A)* **1968,** 504.
(24) Labinger, J. A.; Herring, A. M.; Bercaw, J. E. *J. Am. Chem. Soc.* **1990**, *112*, 5628.
(25) Sen, A.; Lin, M. R.; Kao, L.-C.; Hutson, A. C. *J. Am. Chem. Soc.* **1992**, *114*, 6385.
(26) Shi, M. *J. Chem. Res.−S* **1998**, 592.
(27) Pouchert, C. J. *The Aldrich Library of FT-IR Spectra*; Aldrich Chemicals: Milwaukee, WI, 1983; Vol. 1, pp 238, 248, 697.

$\times$ $6H_2O$ with THF in HPS is expected to fill the HPS nanocavities with a mixture composed of Pt complexes and residues of the products from THF oxidation.

In marked contrast, addition of $H_2PtCl_6 \times 6H_2O$ to ML, followed by 24 h of agitation and subsequent ML evaporation, does not yield any chemical changes, according to FTIR analysis. In this case, we conclude that both H_2PtCl_6 and ML remain unchanged. This observation is consistent with the reported[25] susceptibility of alcohols to oxidation in the presence of a mixture of Pt(II) and Pt(IV): oxidation becomes increasingly more difficult as the length of the alkyl chain decreases. It must be remembered, however, that incorporation of platinic acid within HPS in ML is accompanied by the reduction of Pt(IV) to Pt(II), as evidenced by XPS and confirmed by visual observations (i.e., the HPS powder darkens). This result corroborates our earlier hypothesis that HPS serves as a reducing agent for Pt(IV) and is most likely oxidized, presumably by the formation of hydroxyl groups.[21,22] According to the FTIR spectrum of metal-free HPS, HPS contains a small concentration of double bonds that can easily coordinate with a Pt complex. The presence of a signal at 330 cm^{-1} in the far-IR spectrum of the HPS-Pt-ML specimen suggests the formation of a *trans*-$PtCl_2L_2$ complex,[28] where L here denotes a functionality (i.e., a double bond or hydroxyl group) belonging to HPS. While complexation of Pt(II) species with alcohols in solution has been documented,[29] such complexes have not been isolated. It is therefore possible that the size restrictions of the HPS nanocavities facilitate complex formation and stabilization.

According to TEM analysis, the HPS-Pt-THF and HPS-Pt-ML specimens contain no metal nanoparticles with a diameter exceeding 0.5 nm (the estimated resolution of the microscope). Electron micrographs of the HPS-Pt samples collected after the precursor samples were reduced with H_2 are presented in Figure 3 and clearly reveal the existence of small Pt nanoparticles possessing mean diameters of 1.3 ± 0.3 nm for HPS-Pt-THF (Figure 3a) and 1.4 ± 0.3 nm for HPS-Pt-ML (Figure 3b). The size histograms displayed in Figure 4 show that both samples exhibit maxima at 1.2 nm for single nanoparticles. Note that the H_2-reduced HPS-Pt-ML specimen also consists of nanoparticle aggregates ranging in equivalent diameter from 2.4 to 4.0 nm. Results obtained from XRD are included in Figure 5. Since HPS-Pt-THF is an amorphous material, its XRD pattern (not shown) is featureless. The scattering pattern of the reduced HPS-Pt-THF nanocomposite is consistent with the presence of well-defined Pt(0) particles possessing a mean diameter of about 1−2 nm, which is in good quantitative agreement with the TEM results.

In summary, we propose the following mechanism to explain the production of Pt-containing HPS. Upon sorption of the H_2PtCl_6 solution in THF by HPS and subsequent THF evaporation, the solution becomes sufficiently concentrated so that the oxidation−reduction reactions described earlier occur in the HPS nanocavities. Both HPS and THF are oxidized, whereas the Pt compound is reduced[24,25] to a Pt(II) complex. Since the complex effectively fills the HPS nanocavities, H_2 reduction of HPS-Pt-THF results in the formation of Pt nanoparticles with a mean diameter of about 1.3 nm. This size is consistent with the contraction of Pt complex clusters after ligand removal and the formation of a metallic phase. To put this size scale in perspective, the formation of Co nanoparticles in HPS yields nanoparticles typically measuring about 2 nm in diameter. In this case, nanoparticles form upon the thermal decomposition of metal complexes at 200 °C. While thermal decomposition is expected to facilitate atomic or tiny cluster migration, the size of the Co nanoparticles remains primarily governed by the size of the HPS nanocavities over a wide range of Co concentrations. In the present work, H_2 reduction of the Pt precursor greatly lowers the probability of such intercavity migration at ambient temperature, in which case the nanoparticle size is strictly limited by the source of Pt atoms in each cavity.

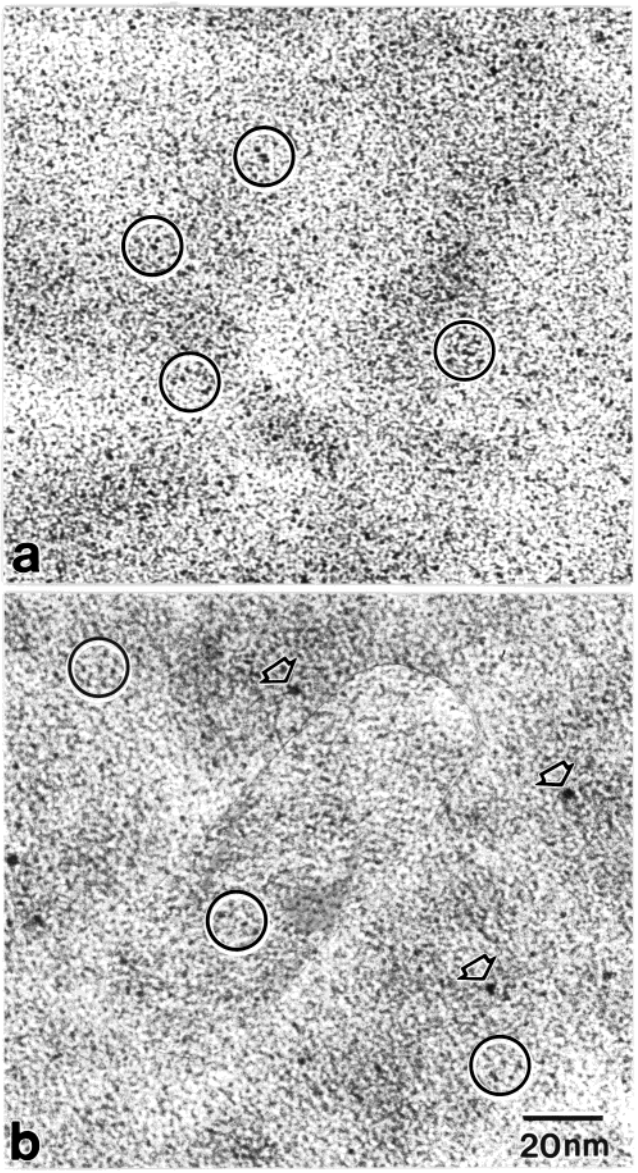

Figure 3. Transmission electron micrographs of (a) HPS-Pt-THF and (b) HPS-Pt-ML after H_2 reduction. Groups of single Pt nanoparticles are highlighted by circles, whereas nanoparticle aggregates in part b are identified by arrowheads.

Thus, the amount of precursor (Pt complex), as well as the size of the nanoparticles formed from the Pt atoms, is determined exclusively by the HPS cavity size. On the basis of the van der Waals radius of Pt (0.17 nm) and the corresponding atomic volume (0.0213 nm^3), it immediately follows that a spherical Pt nanoparticle with a diameter of 1.3 nm (and a volume of 1.15 nm^3) should contain about 54 Pt atoms and should have an effective surface area of 5.30 nm^2. According to these results, 1 g of HPS-Pt-THF (with a composition of 7.51 wt % Pt from Table 1) contains 3×10^{18} nanoparticles with a total surface

(28) Adams, D. M.; Chatt, J.; Gerratt, J.; Westland, A. D. *J. Chem. Soc.* **1964**, 734.

(29) Belluco, U.; Cattalin, L.; Basolo, F.; Pearson, R. G.; Turco, A. *J. Am. Chem. Soc.* **1965**, *87*, 241.

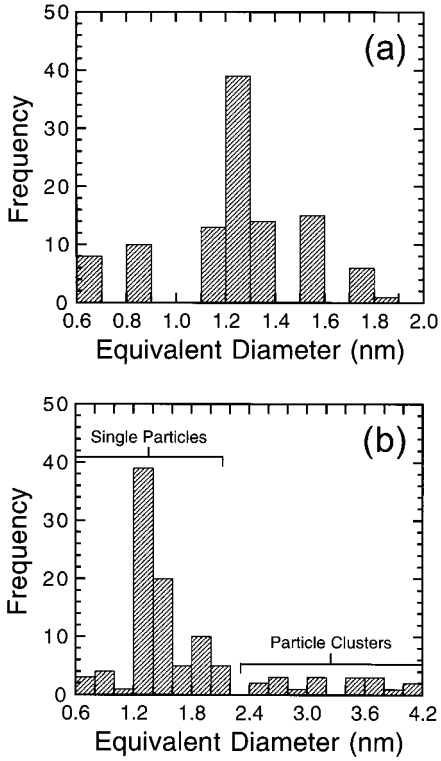

Figure 4. Particle size histograms derived from TEM images such as those presented in Figure 3 for (a) HPS-Pt-THF and (b) HPS-Pt-ML.

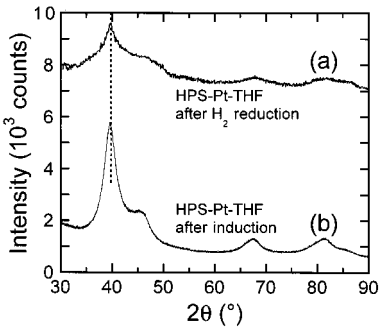

Figure 5. X-ray diffraction patterns collected from (a) H_2-reduced HPS-Pt-THF and (b) HPS-Pt-THF after the induction period. The pattern in part a has been shifted vertically (by 6000 counts) to facilitate scrutinization.

area of 15.9 m^2/g. For comparison, complementary studies[30−32] have shown that stable Ru, Rh, Pd, and Pt clusters containing 55 atoms (the characteristic number of atoms to account for 2 layers of atoms covering a central atom) can be prepared if they are stabilized by ligands such as phosphines. We hasten to point out that the diameter of a single Pt_{55} cluster is reported[30] to be about 1.3 nm, which coincides embarrassingly well with the size of the Pt nanoparticles obtained in the present study. Thus, HPS possesses a unique ability to stabilize an enormous population of Pt clusters, each composed of 76% surface atoms.[32]

In the case of the HPS-Pt-ML material, the situation is slightly different. Since ML does not reduce Pt(IV) during evaporation, all the chemical changes in HPS-Pt-ML are induced solely by the polymer matrix. *Trans*-$PtCl_2L_2$ complexes apparently form within the HPS nanocavities due to specific interactions with HPS functionalities (e.g., double bonds and hydroxyl groups), but a significant fraction of Pt(IV) species remains in the polymer. After H_2 reduction, the precursor complex transforms into Pt nanoparticles. The existence of relatively large particles may be attributed to the higher Pt concentration relative to the H_2-reduced HPS-Pt-THF specimen (see Table 1). As discussed elsewhere,[14] a limiting concentration appears to exist (8 wt % for Co) below which nanoparticle size is not sensitive to the loading level of the metal compound. At higher concentrations, the formation of larger nanoparticles or nanoparticle aggregates (as seen in Figure 3b) ensues.

Catalytic Properties of Pt-Containing HPS. In the direct oxidation of L-sorbose to 2-keto-L-gulonic acid (according to Scheme 1), four specimens have been examined: HPS-Pt-ML and HPS-Pt-THF before and after H_2 reduction. To ascertain the optimal conditions favoring L-sorbose oxidation with HPS-Pt-THF, the following reaction parameters have been varied: catalyst concentration (C_c) from 0.007 to 0.027 M Pt, L-sorbose concentration (C_0) from 0.22 to 0.50 M, $NaHCO_3$ concentration (C_{NaHCO_3}) from 0.22 to 0.50 M, reaction temperature (T) from 60 to 80 °C, reaction time (t) from 180 to 220 min, oxygen flow rate (V_O) from 7.5×10^{-6} to 20×10^{-6} m^3/s, and stirring rate from 200 to 1000 rpm. Several parameter relationships are readily established from the data collected during the course of this study and are presented in Table 2. For example, a decrease in V_O (compare runs 2 and 8) lowers both the L-sorbose conversion and selectivity. This trend is explained by the decreased amount of oxidizing agent present and by diffusion limitations that become non-negligible at reduced flow rates (O_2 bubbling provides additional mixing). Conversely, an increase in V_O (see runs 2 and 9) results in a lower final pH due to accumulation of acid, which in turn slows down the reaction. In this case, L-sorbose conversion and selectivity likewise decrease. As identified above, a reduction in the stirring rate from 1000 to 200 rpm also promotes a decrease in conversion and selectivity due to the onset of diffusion limitations (see runs 2 and 12).

Comparison of the runs 2, 13, and 14 in Table 2 reveals that L-sorbose conversion is incomplete at $t = 180$ min. An increase in t to 220 min yields 100% conversion, but a pronounced decrease in selectivity due to the formation of 2-keto-L-gulonic acid oxidation products. A similar situation occurs when C_c is increased (as in runs 2 and 3) and when C_0 is decreased (as in runs 2 and 4). In marked contrast, opposite changes in C_c (runs 2 and 1) and C_0 (runs 2 and 5) result in incomplete L-sorbose conversion. From the data corresponding to runs 2, 6, and 7, an increase or decrease in C_{NaHCO_3} changes the pH of the reaction medium, which has an overall negative effect on the selectivity of the transformation of L-sorbose to 2-keto-L-gulonic acid.[33] Temperature control is another adjustable parameter that must be considered in the direct oxidation of L-sorbose. A reduction in T by 10 °C (see runs 2 and 10) yields a decrease in L-sorbose conversion, whereas an increase in T by 10 °C (see runs 2 and 11) results in further oxidation of 2-keto-L-gulonic acid. According to the data listed in Table 2, it immediately follows that direct L-sorbose oxidation is very sensitive to changes in the reaction parameters investigated here.

The highest selectivity (98%) at 100% L-sorbose conversion is achieved with the HPS-Pt-THF catalyst under the following set of reaction conditions: $C_c = 0.021$ M Pt, $C_0 = 0.42$ M, $C_{NaHCO_3} = 0.42$ M, $T = 70$ °C, $V_O = 14 \times 10^{-6}$ m^3/s, stirring rate = 1000 rpm, and $NaHCO_3$ added continuously for 180 min.

(30) Schmid, G.; Huster, W. *Z. Naturforsch. (B)* **1986,** *41*, 1028.
(31) Barreteau, C.; Desjonquères, M. C.; Spanjaard, D. *Eur. Phys. J. D* **2000**, *11*, 395.
(32) Nützenadel, C.; Züttell, A.; Chartouni, D.; Schmid, G.; Schlapbach, L. *Eur. Phys. J. D* **2000**, *8*, 245.

Table 2. Reaction Activity and Selectivity of HPS-Pt-THF in the Direct Oxidation of L-Sorbose[a]

run[b]	C_c (M)	C_0 (M)	C_{NaHCO_3} (M)	$V_O \times 10^6$ (m^3/s)	T (°C)	t (min)	pH[c]	conversion (%)	yield (%)	selectivity (%)
1	0.007	0.42	0.42	14.0	70	200	8.3	76	37	76.0
2	0.021	0.42	0.42	14.0	70	200	6.5	100	98	98
3	0.027	0.42	0.42	14.0	70	200	5.4	100	71	71.0
4	0.021	0.22	0.22	14.0	70	200	4.9	100	68	68.0
5	0.021	0.50	0.50	14.0	70	200	8.9	82	61	74.4
6	0.021	0.42	0.40	14.0	70	200	6.1	79	52	65.8
7	0.021	0.42	0.44	14.0	70	200	9.2	68	30	44.1
8	0.021	0.42	0.42	7.5	70	200	8.8	71	35	49.3
9	0.021	0.42	0.42	20.0	70	200	4.7	95	58	61.1
10	0.021	0.42	0.42	14.0	60	200	9.4	68	24	35.3
11	0.021	0.42	0.42	14.0	80	200	8.5	100	15	15.0
12[d]	0.021	0.42	0.42	14.0	70	200	9.2	74	41	55.4
13	0.021	0.42	0.42	14.0	70	180	7.7	85	83	97.7
14	0.021	0.42	0.42	14.0	70	220	5.9	100	70	70.0

[a] $NaHCO_3$ is loaded continuously over 180 min. [b] Stirring rate is 1000 rpm. [c] Final pH values. [d] Stirring rate is 200 rpm.

As expected from earlier findings,[33] gradual loading of the alkaline agent ensures higher selectivity than one-shot loading because it provides better control over the pH of the reaction medium. Since the oxidation rate is effectively limited by the rate of $NaHCO_3$ addition, continuous loading is not employed in the kinetic experiments described in the next section. While the highest selectivity of the HPS-Pt-THF catalyst is 98%, the highest selectivity of the HPS-Pt-ML catalyst, on the other hand, does not exceed 40%. This significant difference in selectivity can be explained in terms of the different catalytic species present. After H_2 reduction, comparable Pt nanoparticles form in both materials, but their selectivity does not exceed 88−90% at 100% L-sorbose conversion. While we recognize that other explanations for such decreased selectivity may exist, we attribute this observation to a difference in the surface properties of Pt nanoparticles formed by H_2 versus in situ reduction. According to the data presented here, this difference appears sufficient to alter the sorption−desorption equilibria of the L-sorbose, oxygen, and 2-keto-L-gulonic acid.

The kinetic characteristics of selective L-sorbose oxidation have been studied with regard to HPS-Pt-THF and HPS-Pt-ML catalysts in which the substrate/catalyst concentration ratio ($q = C_0/C_c$) has been varied as follows: 12.1 to 32.2 mol/mol Pt for HPS-Pt-THF and 10.2 to 30.1 mol/mol Pt for HPS-Pt-ML. These experiments have been conducted with an O_2 flow rate of 14×10^{-6} m^3/s and a stirring rate of 1000 rpm at 70 °C. As discussed above, the reaction medium is charged with a single shot of the alkaline agent (in an equimolar amount with respect to the L-sorbose) before the beginning of the reaction. The dependence of L-sorbose conversion on reaction time is presented in Figure 6 and demonstrates that an increase in q (or, alternatively, an increase in C_0 at constant C_c) promotes an increase in reaction time (t), which is typical for most catalysts. These kinetic curves also reveal the existence of an induction period of about 100 min, during which time L-sorbose conversion is negligible.

A sample of the HPS-Pt-THF catalyst collected after the induction period has been isolated and subjected to examination by XRD, TEM, and XPS. The XRD pattern acquired from this material indicates the presence of Pt crystallites possessing a mean diameter of ca. 4 nm, along with some unresolved structure that might be assigned to amorphous Pt nanoclusters (see Figure 5b). An electron micrograph of this sample (Figure 7) shows the coexistence of small nanoparticles with a mean diameter approaching the resolution of the microscope (0.5 nm) and larger particles with a mean diameter of up to 6.0 nm. The

(33) Kiyoura, T. U.S. Patent No. 4, 599,446, July 8, 1986.

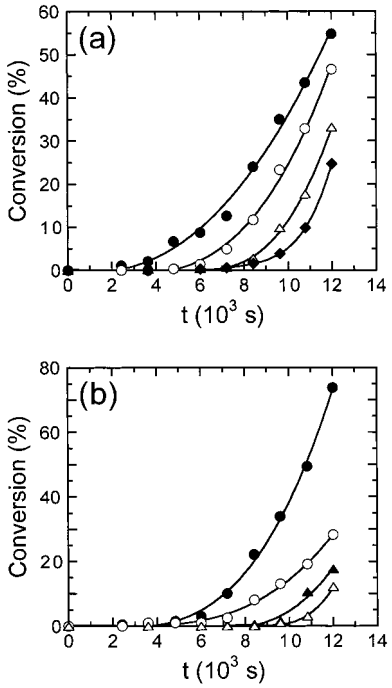

Figure 6. Dependence of L-sorbose conversion on reaction time (t) in the presence of (a) HPS-Pt-THF and (b) HPS-Pt-ML at different L-sorbose concentrations (C_0, in M): 0.05 (●), 0.11 (○), 0.16 (▲), 0.22 (△), and 0.32 (♦). Parts a and b do not include every C_0 for which symbols have been assigned. The solid lines are guides for the eye.

overall mean diameter of the nanoparticles in this specimen is measured to be 1.8 ± 1.1 nm. According to the corresponding histogram provided in Figure 8, the size distribution of the nanoparticles exhibits a maximum in the vicinity of 1.0 nm and becomes fairly continuous thereafter. If we assign those nanoparticles with a diameter less than or equal to 2.0 nm as representative of the initial nanoparticles in the system (see Figure 4a) and those larger than 2.0 nm as enlarged due to L-sorbose oxidation, then the mean diameter and fraction of initial nanoparticles are 1.2 ± 0.5 nm and 71%, respectively.

The population of enlarged particles measures 3.2 ± 0.9 nm in diameter, in reasonably good agreement with the XRD results. Formation of these nanoparticles in this catalyst can be explained by two concurrent events: (i) slow, but continued, reduction by L-sorbose and (ii) facilitated diffusion due the swollen state of HPS during the oxidation reaction in aqueous media. Since the first consideration should hinder nucleation, fewer nuclei and, generally speaking, larger particles are anticipated to develop.[5] The image in Figure 7, however, displays a large

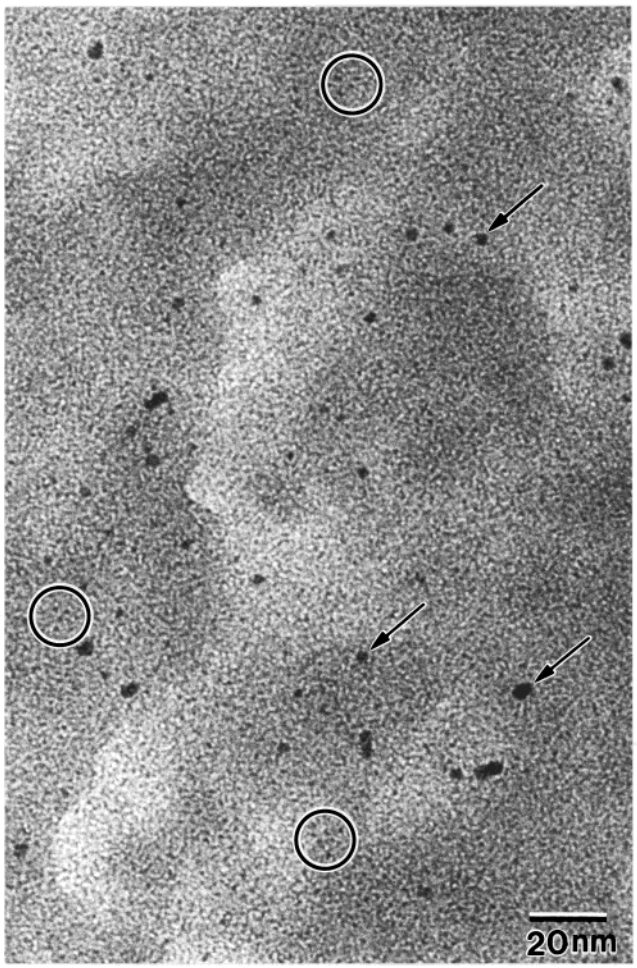

Figure 7. TEM image of HPS-Pt-THF after the induction period during the direct oxidation of L-sorbose in aqueous medium. Groups of single Pt nanoparticles are highlighted by circles, whereas substantially enlarged nanoparticles are identified by arrows.

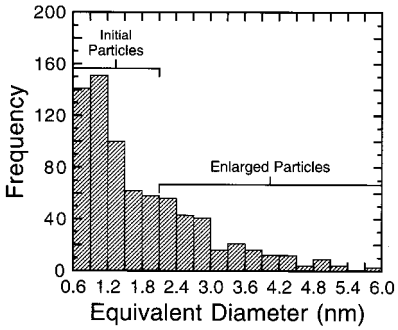

Figure 8. Particle size histogram generated from TEM images such as the one displayed in Figure 7 for HPS-Pt-THF after the induction period.

population of the initial (small) nanoparticles, thereby indicating that the nucleation rate of the nanoparticles does not significantly influence their size. In this case, nanoparticle growth is restricted by both the size of the HPS nanocavities and strong chemical interactions with L-sorbose. On the basis of this conclusion, it follows that the presence of enlarged nanoparticles in this catalyst is most likely the result of the second consideration: facilitated aggregation of small Pt nanoclusters in water-swollen HPS. This explanation is furthermore consistent with the greater population of enlarged nanoparticles, and correspondingly lower activity, observed in the HPS-Pt-ML catalyst after its induction period (data not shown).

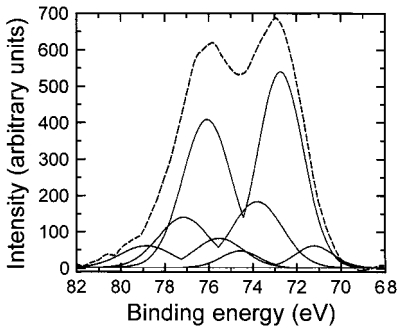

Figure 9. XPS spectrum of HPS-Pt-THF after the induction period of the catalyst during the direct oxidation of L-sorbose in aqueous media. The experimental data are displayed as dashed lines, whereas deconvolution fits are shown as solid lines.

According to the XPS data provided in Figure 9, the Pt $4f_{7/2}$ binding energy changes from 73.6 to 72.4.eV after the induction period in the HPS-Pt-THF catalyst. Deconvolution of this spectrum reveals four different species with different binding energies. While one of them possesses a Pt $4f_{7/2}$ binding energy of 71.3 eV and can be ascribed to Pt(0), additional species with higher binding energies also appear to exist, which is contrary to the XRD results indicating the presence of Pt(0) nanoparticles. One possible explanation for this apparent contradiction is that L-sorbose partially reduces Pt(II) to Pt(0), in which case mixed-valence nanoparticles form. Alternatively, the presence of "oxidized" Pt species may reflect the strong chemical interaction between the surface atoms of the Pt nanoparticles and 2-keto-L-gulonic acid. Such interaction can strongly change the binding energy of Pt. In both scenarios, catalytic species are undoubtedly formed in situ during the induction period. Therefore, HPS appears to serve two crucial roles: one as a support for the Pt catalyst during L-sorbose oxidation and the other as the nanostructured matrix responsible for controlling nanoparticle growth.

As is evident from the data listed in Table 2, the reaction temperature constitutes an important reaction parameter in the present study. Here, we examine the effect of T on the kinetics of L-sorbose oxidation over the range 60−80 °C (the conditions employed in the previous kinetic experiments are retained). Resultant data are presented in Table 3 and show that an increase in T promotes an increase in the rate of L-sorbose oxidation. It is interesting to note that the reaction selectivity decreases markedly for both the HPS-Pt-THF and HPS-Pt-ML catalysts at 80 °C. A reasonable explanation for this observation is further oxidation of 2-keto-L-gulonic acid under the reaction conditions (which eventually results in the formation of CO_2). At the highest selectivity of the HPS-Pt-THF catalyst measured in this work (98% at 100% conversion), the value of the turnover frequency (TOF) is found to be 5.4×10^{-4} [mol/mol Pt·s], which is comparable in magnitude to previously reported[19] data at significantly lower conversions.

The T dependence of L-sorbose oxidation can be further examined if Arrhenius behavior is obeyed. To ascertain the applicability of the Arrhenius equation in the present work, we have measured the reaction time yielding 10% L-sorbose conversion ($\tau_{0.1}$). A graphical representation of $1/\tau_{0.1}$ as a function of $1/T$ is displayed on semilogarithmic coordinates in Figure 10 and demonstrates that Arrhenius behavior is exhibited by both catalysts over the temperature range investigated. Regression of the data shown in this figure yields apparent activation energy (Q) values of 39 ± 3 and 41 ± 7 kJ/mol for HPS-Pt-THF and HPS-Pt-ML, respectively. Values of the frequency factor (υ_0) derived from the ordinate intercept would

Table 3. Influence of Temperature on L-Sorbose Oxidation with HPS-Pt-THF and HPS-Pt-ML[a]

	temperature[b] (°C)				
reaction outcome	60	65	70	75	80
L-sorbose conversion (%)	15.0/15.5[b]	22.0/18.5	47.0/26.0	63.0/38.0	82.0/75.0
2-keto-L-gulonic acid (%)	12.0/10.5	19.0/15.3	45.0/24.5	55.0/33.0	59.0/56.3
selectivity (%)	80.0/67.7	86.4/82.7	95.7/94.2	87.3/86.8	72.0/75.1
TOF × 10^4 (mol/mol Pt•s)	1.7/1.2	2.5/1.9	5.4/2.8	7.2/3.8	9.4/6.5

[a] Reaction conditions: $V_O = 14 \times 10^{-6}$ m^3/s; $NaHCO_3$ is charged one-shot at the beginning of the reaction; $C_0 = 0.107$ M; $q = 13.8$ mol/mol Pt; $t = 200$ min. [b] The data are presented in the format of HPS-Pt-THF/HPS-Pt-ML.

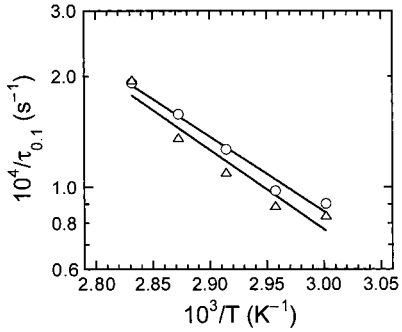

Figure 10. The temperature dependence of the reaction time yielding 10% conversion of L-sorbose in the presence of HPS-Pt-THF (○) and HPS-Pt-ML (△). The solid lines denote regressed fits of the Arrhenius equation and yield the activation energy (Q) values listed in the text.

Table 4. Activity and Selectivity of HPS-Pt-THF after Repeated Catalytic Cycles[a]

no. of catalytic cycles	TOF × 10^4 (mol/mol Pt•s)	selectivity (%)
1	5.4	95.7
7	5.3	95.0
15	5.5	95.1

[a] See Table 3 ($T = 70$ °C) for the reaction conditions.

provide a measure of the number of collisions or active centers on the surface of a catalyst surface,[34] but suffer from inaccuracy due to scatter in the data. Since both catalysts possess almost identical activation energies, we infer that the number of active catalytic centers is greater for HPS-Pt-THF than HPS-Pt-ML to explain the significantly higher activity of the HPS-Pt-THF catalyst. This result is consistent with the greater fraction of large nanoparticles, with lower surface area, in the HPS-Pt-ML material.

In addition to selectivity and activity, another important feature of any promising catalyst is the stability of its catalytic properties. Unfortunately, catalysts often lose their activity after only two or three repeated uses, typically due to either loss of the catalytic metal[35] or contamination of the catalytic surface by reaction products.[36] As is seen from the data tabulated in Table 4, neither the activity nor the selectivity of the HPS-Pt-THF catalyst deteriorates even after 15 catalytic cycles. This result demonstrates that nanoparticles can exhibit remarkably stable catalytic properties. Such stability is attributed to what we refer to as "double protection", in which (i) the location of the nanoparticles within HPS nanocavities of comparable size prevents leaching of catalytic metal; and (ii) chemical interaction of the nanoparticle surface with 2-keto-L-gulonic acid avoids surface contamination.

(34) Sakakini, B. H.; Verbrugge, A. S. *J. Chem. Soc., Faraday Trans.* **1997**, *93*, 1637.
(35) Bakos, I.; Mallat, T.; Baiker. A. *Catal. Lett.* **1997**, *43*, 201.
(36) Schuurman, Y.; Kuster, B. F. M.; van der Wiele, K.; Marin, G. B. *Appl. Catal. A−Gen.* **1992**, *89*, 47.

Experimental Section

Materials. The HPS was synthesized according to the procedure described in detail elsewhere,[12] whereas $H_2PtCl_6 \times 6H_2O$ and sodium hydrogencarbonate ($NaHCO_3$) were obtained from Reakhim (Moscow, Russia). Reagent-grade tetrahydrofuran (THF) and methanol (ML) were purchased from Aldrich and used as received, as was the L-sorbose from Fluka. Water was purified with a Milli-Q water purification system.

HPS-Pt Preparation. Particles of HPS were inserted into a Schlenk tube capped with a rubber septum. Following evacuation at 1.5 mbar, the tube was filled with Ar. In a typical synthesis, 0.4 g of H_2PtCl_6 was dissolved in 4 mL of THF or ML, which promoted complete swelling of 1 g of HPS without excess solvent. The solution was subsequently added to the Schlenk tube by syringe through the rubber septum. After the HPS was allowed to swell for 30 min in the H_2PtCl_6 solution, it was evacuated for 3 days at 1.5 mbar. Table 1 lists elemental analysis data of the resultant HPS-Pt samples, which were later reduced in a steady flow of H_2 for 3 h at ambient temperature.

L-Sorbose Oxidation. The reaction was conducted batchwise in a specially constructed apparatus that permits control over such parameters as the L-sorbose and $NaHCO_3$ concentrations, catalyst concentration, temperature, (pure) oxygen feed rate, and stirring rate. A solution of catalyst and L-sorbose (100 mL) prepared at a predetermined concentration was placed in the temperature-controlled apparatus equipped with a magnetic stir bar and reflux condenser. The rate of oxygen feed was controlled by a rotameter. An equimolar quantity of alkalizing agent ($NaHCO_3$) was fed to the apparatus in one shot or continuously over 180 min (to maintain a constant pH of 7.7) with use of an automatic dispenser. The high stirring rates employed here ensured good mixing without diffusion limitation. Samples of the reaction mixture were periodically removed for analysis. At the end of the experiment, the catalyst was separated by filtration, and the filtrate was analyzed for the presence of L-sorbose and 2-keto-L-gulonic acid. The amount of residual L-sorbose was discerned by gas chromatography (GC) through the use of a "Chrom-5" chromatograph, operated isothermally with a flame-ionization detector and glass column filled with 5% SE-30 on Chromaton N-AW. The quantity of 2-keto-L-gulonic acid was determined by the classical iodometric method of Heyns.[37] For runs 2, 7, and 13 listed in Table 2, the quantity of 2-keto-L-gulonic acid was determined by direct isolation via amine complexation[38] and subsequent transformation to the sodium salt of ascorbic acid,[39] the purity of which (98.5%) was measured at Belgorodvitaminy (Belgorod, Russia) with a "Millichrom 4" HPLC equipped with a UV detector, a PLRS-s 100A solid polymer phase, and a 0.2 M NaH_2PO_4(aq) liquid phase. Each experiment reported here was repeated at least 3 (often 5) times to ensure reproducibility.

Material Characterization. X-ray fluorescence (XRF) measurements were performed with a Zeiss Jena VRA-30 spectrometer (Mo anode, LiF crystal analyzer and SZ detector). Analyses were based on the Co Kα line and a series of standards prepared by mixing 1 g of polystyrene with 10−20 mg of standard compounds. The time of data acquisition was constant at 10 s. Fourier-transform infrared (FTIR) spectra were recorded with a Nicolet spectrometer in the spectral region ranging from 250 to 4000 cm^{-1} at a resolution of 2 cm^{-1}. X-ray diffraction (XRD) measurements were acquired with a Rigaku D/max-

(37) Heyns, K. *Ann. Chem.* **1947**, *558*, 171, 177.
(38) Schaper, M. German Offen. DE 3831070 A1, 1990.
(39) Crawford, T. C.; Crawford, S. A. *Adv. Carbohydr. Chem. Biochem.* **1980**, *37*, 79.

RC diffractometer operated at 12 kV with Cu Kα radiation. X-ray photoelectron spectroscopy (XPS) was conducted with a two-chamber Kratos XSAM-800 spectrometer. Powdered samples were evacuated in the spectrometer for 12 h at $10^{-9}-10^{-10}$ mbar, and spectra were collected in the medium resolution regime at 25 °C. For photoelectron excitation, characteristic Mg Kα radiation ($h\upsilon = 1253.6$ eV) was used. The power of the X-ray gun never exceeded 75 W (15 kV, 5 mA). Transmission electron microscopy (TEM) was performed with a Zeiss EM902 electron spectroscopic microscope operated at 80 kV and an energy loss of 0 eV. Insoluble HPS-Pt powders were embedded in epoxy resin and subsequently microtomed at ambient temperature. Images of the resulting thin sections (ca. 50 nm thick) were collected on plate negatives, digitized at 600 dpi, and analyzed with the Adobe Photoshop software package and the companion Image Processing Toolkit. Solid-state ^{13}C magnetic resonance (NMR) spectra were collected with a 4.0 mm Bruker Magic Angle Spinning Probe in a Bruker Avame DSX spectrometer. Data were obtained by using cross polarization from protons (4 μs proton $\pi/2$ pulse, 500 μs contact time) under 12.000 kHz magic angle spinning. Two-pulse phase modulation (TPPM) decoupling was employed during acquisition.[40]

Conclusions

A robust strategy for synthesizing Pt-containing hyper-cross-linked PS is described. The accumulation of Pt(II) complexes, as well as subsequent Pt nanoparticle formation, is effectively restricted by the size of the HPS nanocavities. After H_2 reduction in dry, solid polymer, the nanoparticles possess a narrow size distribution and a mean diameter of 1.3−1.4 nm. Following the reduction of Pt(II) species during the induction period of catalytic L-sorbose oxidation, the nanoparticles exhibit a significantly broader size distribution. The small nanoparticles possess a mean diameter of about 1.2 nm and are restricted in size by the HPS nanocavity and chemical interaction with 2-keto-L-gulonic acid. Enlarged nanoparticles measuring up to 6.0 nm in diameter and having a mean diameter of about 3.2 nm form due to aggregation in water-swollen HPS. The catalytic activity and selectivity of these nanocomposite materials have been measured under a wide variety of reaction conditions. These catalysts exhibit high selectivity (98% at 100% conversion) and remarkably stable catalytic properties that remain practically unchanged after 15 catalytic cycles. In this regard, the nanostructured HPS matrix serves as both a nanoscale reactor and catalyst support to (i) restrict the growth of the nanoparticles, (ii) prevent leaching of the nanoparticles, and (iii) ensure a high degree of chemical interaction.

Acknowledgment. L.M.B., S.N.S., P.M.V., V.G.M., N.V.L., and E.M.S. were supported by the Russian Foundation for Basic Research (Grant No. 01-03-32937) and the NATO Science for Peace Program (SfP-974173-Colloidal Catalysts).

JA0107834

(40) Auger, M.; Lakshmi, K. V.; Griffin, R. G. *J. Chem. Phys.* **1995**, *103*, 6951.